

PAPER • OPEN ACCESS

Nondipolar photoelectron angular distributions from fixed-in-space N₂ molecules













To cite this article: D V Rezvan *et al* 2024 *J. Phys. B: At. Mol. Opt. Phys.* **57** 145101

View the [article online](#) for updates and enhancements.

You may also like

- [Nondipole effects in laser-assisted electron scattering](#)
Simon Vendelbo Bylling Jensen and Lars Bojer Madsen
- [Which Component of Solar Magnetic Field Drives the Evolution of Interplanetary Magnetic Field over the Solar Cycle?](#)
Minami Yoshida, Toshifumi Shimizu and Shin Toriumi
- [Nondipole photoelectron momentum shifts in strong-field ionization with mid-infrared laser pulses of long duration](#)
Mads Middelhede Lund and Lars Bojer Madsen

Nondipolar photoelectron angular distributions from fixed-in-space N₂ molecules

D V Rezvan¹ , A Pier² , S Grundmann² , N M Novikovskiy¹ , N Anders² ,
M Kircher² , N Melzer² , F Trinter^{3,4} , M S Schöffler² , T Jahnke^{5,6} , R Dörner² 
and Ph V Demekhin^{1,*} 

¹ Institut für Physik und CINSaT, Universität Kassel, Heinrich-Plett-Str. 40, 34132 Kassel, Germany

² Institut für Kernphysik, Goethe-Universität Frankfurt, Max-von-Laue-Str. 1, 60438 Frankfurt am Main, Germany

³ Molecular Physics, Fritz-Haber-Institut der Max-Planck-Gesellschaft, Faradayweg 4-6, 14195 Berlin, Germany

⁴ FS-PETRA-S, Deutsches Elektronen-Synchrotron (DESY), Notkestr. 85, 22607 Hamburg, Germany

⁵ Max-Planck-Institut für Kernphysik, Saupfercheckweg 1, 69117 Heidelberg, Germany

⁶ European XFEL, Holzkoppel 4, 22869 Schenefeld, Germany

E-mail: demekhin@physik.uni-kassel.de

Received 30 March 2024, revised 8 May 2024

Accepted for publication 14 June 2024

Published 26 June 2024



CrossMark

Abstract

We investigate experimentally and theoretically the N 1s photoionization of fixed-in-space N₂ molecules at a photon energy of 880 eV. In our experiment, we employed circularly polarized synchrotron radiation for the photoionization and coincident electron and fragment-ion detection using cold target recoil ion momentum spectroscopy. The accompanying angle-resolved calculations were carried out by the multichannel single-center method and code within the frozen-core Hartree–Fock approximation. The computed emission distributions exhibit two distinct features along the molecular axis, which are the results of a superposition of the direct and nearest-neighbor scattering amplitudes for the photoemission from two nitrogen atoms. In the electric-dipole approximation, these peaks are symmetric with respect to both nitrogen atoms. Including nondipole (retardation) effects in the calculations results in a simultaneous increase and decrease of the scattering peaks towards the nitrogen atoms pointing in the forward and backward directions along the light propagation, respectively. These theoretical findings are in agreement with our experimental findings.

Keywords: photon interactions with molecules, inner-shell photoionization, molecular-frame angular distributions, nondipole (retardation) effects

* Author to whom any correspondence should be addressed.



Original Content from this work may be used under the terms of the [Creative Commons Attribution 4.0 licence](https://creativecommons.org/licenses/by/4.0/). Any further distribution of this work must maintain attribution to the author(s) and the title of the work, journal citation and DOI.

1. Introduction

In a majority of theoretical studies of light–matter interaction, it is well justified to employ the electric-dipole approximation, which neglects the spatial dependence of the radiation plane wave and thus its retardation. Nevertheless, a continuous enhancement of the experimental detection techniques and the refinement of their precision provides unambiguous proof of a breakdown of the electric-dipole approximation [1]. In x-ray photoionization of atoms and randomly oriented molecules, nondipole effects induce a notable dependence of the laboratory-frame photoelectron angular distributions on the direction of the light propagation [2–4], and their influence increases with increasing photon energy. If the photoemission from fixed-in-space molecules is considered (see, e.g. studies of molecular-frame photoelectron angular distributions [5–7]), geometrical properties of ionized targets start to play a dominant role in the formation of the angular distributions. Contrary to the nondipolar effects, the role of such multiple-scattering effects caused by the molecular potential decreases as the photon energy is increased.

For fixed-in-space molecules, a superposition of effects caused by the molecular potential on one side and nondipole contributions due to the light retardation on the other side may induce intricate asymmetries in the photoelectron emission distributions [8]. One of such asymmetries was reported in our recent experimental and theoretical study of fixed-in-space CO molecules ionized by photons with an energy of 905 eV [9]. On the one hand, molecular-frame angular distributions of high-energy photoelectrons exhibit a distinct nearest-neighbor scattering peak pointing from the emitting atom towards its neighbor (scatterer) [10–13]. On the other hand, the nondipole contributions introduce a notable forward-backward asymmetry with respect to the light propagation direction, typically with more photoelectrons being emitted along the light propagation direction [14, 15] than in the opposite direction. As a consequence of these two effects, the nearest-neighbor scattering peak in our study [9] was notably increased (decreased) if the scatterer atom was pointing in the forward (backward) direction with respect to the light propagation.

In our present work, we perform a joint theoretical and experimental study of similar nondipole-induced asymmetries in the angular emission distribution from fixed-in-space N₂ molecules and discuss two new aspects. Firstly, for homonuclear molecules, there are two nearest-neighbor scattering peaks for the photoemission from two nitrogen atoms. As a consequence, they are simultaneously present in the emission distribution with equal strengths (within the electric-dipole approximation), pointing in two opposite directions along the molecular axis [10, 12, 16]. Thereby, the two aforementioned situations where the scatterer atom points in the forward or in the backward direction with respect to the light propagation are present simultaneously. Secondly, the inner-shell photoionization of homonuclear molecules involves two contributions from the $1\sigma_g$ and $1\sigma_u$ orbitals, and we address the nondipole effects in these contributions separately. For randomly

oriented N₂ molecules, an influence of the nondipole effects on the laboratory-frame angular distribution of inner-shell photoelectrons was studied experimentally and theoretically in [17, 18].

This paper is organized as follows: our experimental and theoretical approaches are outlined in section 2. The results are discussed in section 3. We conclude with a brief summary in section 4.

2. Methods

Our experiment was performed at the soft x-ray beamline P04 of the synchrotron PETRA III [19] at DESY in Hamburg (Germany) and is very similar to that presented in [9]. The synchrotron was operated in the few-bunch timing mode with a bunch spacing of 192 ns. The circularly polarized synchrotron radiation ($\hbar\omega = 880$ eV) was provided by beamline P04 using a 5 m-long APPLE-II undulator. The N₂ molecules were introduced into the chamber in form of a supersonic molecular beam. The coincident detection of the photoelectrons, Auger electrons, and fragment ions created by the Coulomb explosion of the molecules was performed using a COLTRIMS (cold target recoil ion momentum spectroscopy) reaction microscope [20, 21], which is permanently installed at the beamline. All charged particles generated in the photoreaction were guided by homogeneous electric (43.1 V cm⁻¹) and magnetic (36.1 G) fields onto two time- and position-sensitive microchannel plate detectors (with an active area of 80 mm diameter) with hexagonal delay-line position readout.

The ion arm was in total 308 mm long and enhanced by an electrostatic lens yielding time-of-flight and spatial focusing of the fragment ions. The electron arm was in total 66 mm long. It allowed for an efficient detection of high-energy 1s photoelectrons and subsequently emitted Auger electrons with 4π collection solid angle. The particles' impact positions on the detectors and measured flight times provide access to their initial momentum vectors. The difference of the two ionic momentum vectors yields the orientation of the molecular axis in the laboratory frame (e.g. with respect to the light propagation direction). The latter is only valid under the assumption of the axial-recoil approximation [22]. This assumption holds for the reaction channel under investigation, as was demonstrated in [10]. As the photoelectron momentum is measured in coincidence, the electron emission angle in the above-established molecular frame of reference (i.e. relative to the molecular axis) can be retrieved in the experiment.

The present calculations were performed in the frozen-core Hartree–Fock approximation by the stationary single-center (SC) method [23, 24], and, in particular, with its multichannel realization [24]. The bound orbitals of the neutral N₂ molecule were generated at the equilibrium internuclear distance of 2.074 a.u. [25] using the PC GAMESS (US) [26] QC package in the triplet-zeta valence basis set [27]. Those molecular orbitals, decomposed over spherical harmonics with $\ell_{\text{bound}} < 99$ and $m_{\text{bound}} = 0, \pm 1$ with respect to the geometrical center of the molecule, were further used

to create direct and exchange electrostatic Coulomb potentials for the N 1s photoelectrons. In the single-center calculations, the partial photoelectron continuum waves, $\Psi_{\mathbf{k}\ell m}(\mathbf{r})$, with the linear momentum \mathbf{k} and the kinetic energy $\varepsilon = k^2/2$ (which is equal to $\varepsilon = 470.1$ eV for the $1\sigma_g$ and 470.2 eV for the $1\sigma_u$ channels with the respective ionization potentials of 409.9 and 409.8 eV [28]) were described by the $\ell < 50$ and $m < 5$ angular-momentum quantum numbers. The method provides accurate energy-normalized outgoing partial continuum photoelectron waves $\Psi_{\mathbf{k}\ell m}(\mathbf{r})$, as obtained in the field of the molecular potential, with the proper asymptotic behavior [29]. For the considered inner-shell photoionization in the far continuum, electron-correlation effects can be neglected, and even more simplified one-particle approaches (like, e.g. multiple-scattering x-ray photoelectron diffraction theory [30]) provide satisfactory agreement with the experiment. Nevertheless, inter-channel correlations in the continuum were included in the present calculations, and the $1\sigma_g$ and $1\sigma_u$ channels were mixed by the respective Coulomb coupling [31–33].

The angular emission distributions were calculated in the molecular frame of reference in the xz plane, which is spanned by the molecular axis (z axis) and the light propagation direction \mathbf{k}_γ . The latter forms an Euler angle β with the former. Within this geometry, the respective photoemission probability, as a function of the orientation angle β and the emission angle θ , reads [34, 35]:

$$\sigma_\varepsilon(\beta, \theta) = \left| \sum_{\ell m} (-i)^\ell A_{\varepsilon\ell m}(\beta) Y_{\ell m}(\theta, \varphi) \right|^2. \quad (1)$$

Here, $Y_{\ell m}$ are spherical functions and the azimuthal photoemission angle is $\varphi = 0$ and $\varphi = \pi$ for the $x > 0$ and $x < 0$ hemiplanes, respectively. The photoionization amplitudes $A_{\varepsilon\ell m}(\beta)$ for the emission of partial photoelectron continuum waves were computed in the velocity gauge by including the plane wave $e^{i\mathbf{k}_\gamma \cdot \mathbf{r}}$ of the vector potential in the light–matter interaction explicitly:

$$A_{\varepsilon\ell m}(\beta) = \langle \Psi_{\mathbf{k}\ell m}(\mathbf{r}) | e^{i\mathbf{k}_\gamma \cdot \mathbf{r}} (\vec{\varepsilon} \cdot \vec{\nabla}) | \Psi_{1\sigma_{gu}}(\mathbf{r}) \rangle_{\mathbf{r}}. \quad (2)$$

Here, $\vec{\varepsilon}$ is the polarization vector of the circularly polarized light, and the subscript \mathbf{r} indicates an integration over the spatial coordinates in the frame of the molecule.

For circularly polarized light with positive helicity and in the chosen geometry, the following holds:

$$e^{i\mathbf{k}_\gamma \cdot \mathbf{r}} = e^{i\frac{\omega}{c} r (\cos\beta \cos\theta_r + \sin\beta \sin\theta_r \cos\varphi_r)}, \quad (3a)$$

$$(\vec{\varepsilon} \cdot \vec{\nabla}) = -\frac{1}{\sqrt{2}} \left(-\sin\beta \frac{\partial}{\partial z} + \cos\beta \frac{\partial}{\partial x} + i \frac{\partial}{\partial y} \right), \quad (3b)$$

where ω is the photon’s angular frequency and c is the speed of light. Since the initial bound electronic wave functions $\Psi_{1\sigma_{gu}}$ in equation (2) are represented over the known Gaussian basis set $x^a y^b z^c e^{-\alpha r^2}$, the respective partial derivatives over the

molecular Cartesian coordinates in equation (3b) can be taken analytically. Those analytical derivatives were decomposed over spherical harmonics with $\ell_{\text{bound}} < 99$ and $m_{\text{bound}} = 0, \pm 1$ with respect to the molecular center. Afterwards, the photoionization transition amplitudes $A_{\varepsilon\ell m}(\beta)$ were computed by performing the three-dimensional integration over the radial coordinates $\{r, \theta_r, \varphi_r\}$ in equation (2) numerically.

3. Results and discussion

The computed and measured angular emission distributions of the N 1s photoelectrons, obtained for selected orientations of the molecule with respect to the light propagation direction, are depicted in the left and right columns of figure 1, respectively. A sketch of the molecular orientation scheme is shown in figure 1(j). The experimental data include all photoelectrons emitted within an opening angle of $\pm 10^\circ$ out of the picture plane (spanned by the molecular axis and the light propagation direction). The orientation of the molecular axis in the laboratory frame spans intervals of $\beta \pm 10^\circ$ in the panels showing the experimental results. The error bars represent the absolute statistical uncertainties. We do not present experimental results for the molecular orientation angle $\beta = 0^\circ$ as we did not obtain sufficient statistics for this geometry. The calculations are performed in the two ways: in the electric-dipole approximation by setting the plane wave $e^{i\mathbf{k}_\gamma \cdot \mathbf{r}}$ in the transition matrix element (equation (2)) to unity (dipole, blue curves) and beyond this approximation including the plane wave fully (nondipole, red curves). In order to demonstrate a maximal effect, the computed data represent slices of the angular emission distributions in the picture plane.

As one can see from the left panels of figure 1, the photoelectron angular emission distributions, computed in the electric-dipole approximation (blue curves), are symmetric. Indeed, being rotated by 180° , the lower part of each distribution would coincide with its upper part. Thereby, the emission probabilities in the forward and backward hemiplanes, as defined by the light propagation direction (from left to right), are equivalent. The nondipole contributions (red curves), as expected, show a systematic increase of the emission probability in the forward and a corresponding decrease in the backward hemiplane. The effect is most pronounced along the molecular axis, where the emission probabilities exhibit two distinct features. The latter are given by a superposition of the direct and nearest-neighbor scattering amplitudes for the emission from the two equivalent nitrogen atoms [10, 12]. Extended calculations, performed by approximating the plane wave in the transition matrix element (equation (2)) via $e^{i\mathbf{k}_\gamma \cdot \mathbf{r}} \approx 1 + i\mathbf{k}_\gamma \cdot \mathbf{r}$, attribute the main asymmetry effect to the electric-quadrupole and magnetic-dipole expansion terms [9].

Figure 1 illustrates an overall agreement between the shapes of the computed (left panels) and measured (right panels) photoelectron angular emission distributions.

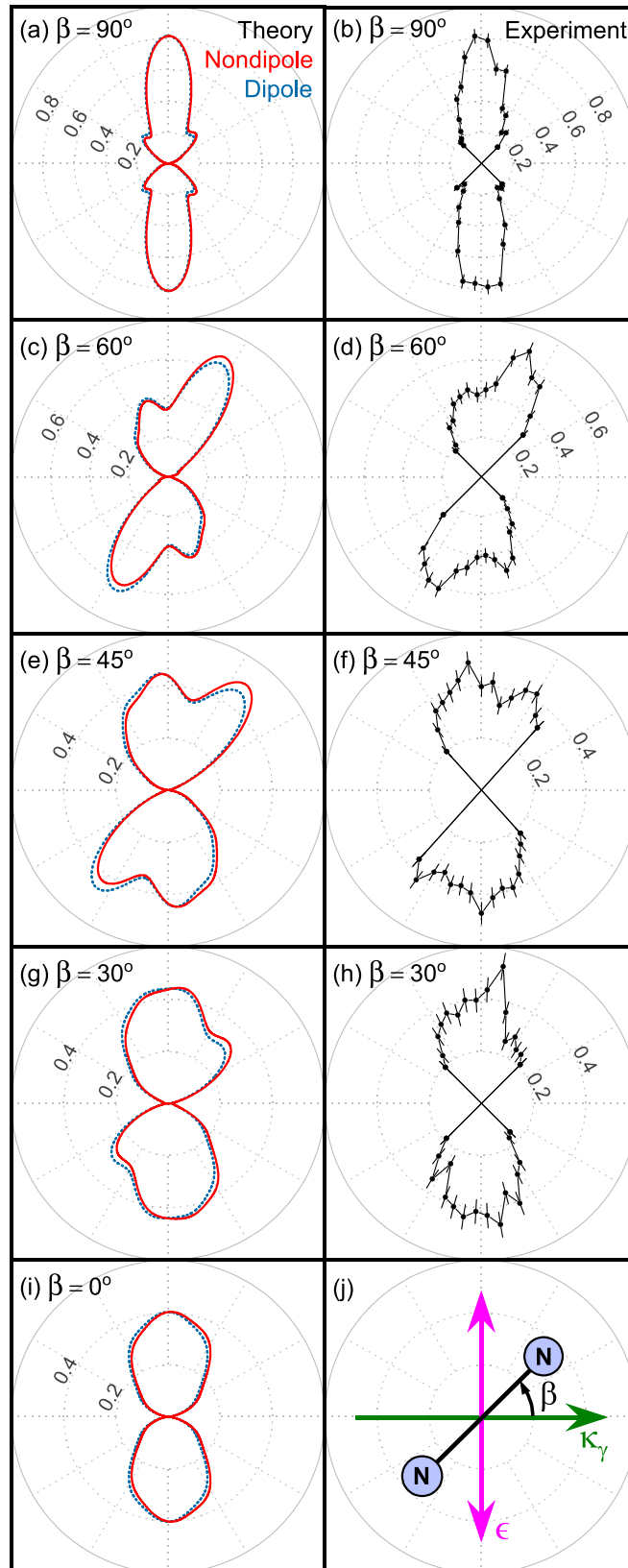


Figure 1. Theoretical dipole and nondipole (left panels) and experimental (right panels) angular emission distribution of the N 1s photoelectrons of N₂ ionized by photons with an energy of 880 eV. The experimental distributions are normalized to the theoretical ones. The relative radial scale is visualized by the dotted concentric circles with inclined numbers. Panel (j): the molecule is oriented in the picture plane at an angle β with respect to the propagation direction (from left to right, green arrow) of the circularly polarized ionizing light (polarization plane, magenta double arrow).

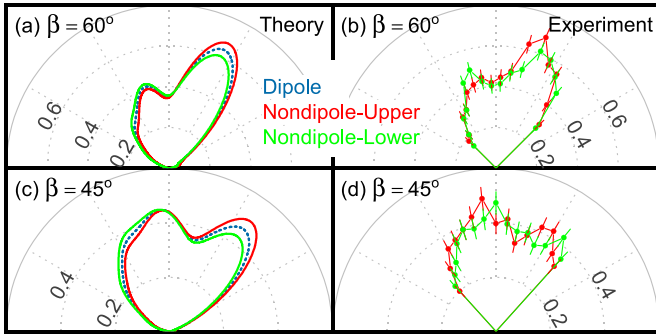


Figure 2. The same as in figure 1 for the two orientation angles $\beta = 60^\circ$ and $\beta = 45^\circ$. Here, the lower part of each distribution (emission angles $180^\circ - 360^\circ$, green curves) is rotated by 180° and compared with the respective upper part (emission angles $0 - 180^\circ$, red curves). See the caption of figure 1 for details on the data representation and the scheme in figure 1(j) for the definition of the molecular orientation angle β .

However, as it is necessary to integrate over finite angular intervals in the experiment (as indicated above), some details in the experimental distributions are washed out, as compared to the theory. Moreover, owing to the solid-angle element, the statistical uncertainties (error bars) grow for smaller molecular orientation angles β significantly. We therefore omitted the measured results for $\beta = 0^\circ$ in figure 1. In order to demonstrate the effect visible in the theory more clearly, we use in figure 2(a) slightly different data representation and compare the theoretical and experimental emission distributions for the two molecular orientation angles $\beta = 60^\circ$ and $\beta = 45^\circ$, for which the effect is largest. In this figure, the upper parts (red curves) of the distributions from figure 1 are shown unchanged, while the lower parts (green curves) are rotated by 180° , such that they can directly be compared with each other. In addition, the symmetric distributions, computed in the electric-dipole approximation, are shown in figures 2(a) and (c) as the blue curves in between the red and green curves, which are equivalent for the upper and lower parts of the dipolar distributions. The emission distribution in figure 2(b), measured for the molecular orientation angle $\beta = 60^\circ$, supports these theoretical findings unambiguously. In particular, this measured distribution is not point-symmetric, as expected in the electric-dipole approximation, and it is systematically enhanced in the forward and reduced in the backward emission direction mainly along the molecular axis (cf red and green curves in figure 2(b)). Unfortunately, owing to the large statistical uncertainties, the distribution in figure 2(d), measured for $\beta = 45^\circ$, cannot be considered as an unambiguous proof of the effect.

Figure 3 shows the breakdown of the computed distributions into the partial $1\sigma_g$ (left panels) and $1\sigma_u$ (right panels) contributions. By symmetry, the $1\sigma_g$ channel (corresponding to a *gerade* *K*-shell hole) exhibits emission probability along the molecular axis. As a consequence, the nondipolar effects are more pronounced in the $1\sigma_g$ channel (cf blue and red curves in each panel). Interestingly, in the $1\sigma_u$ channel (corresponding to an *ungerade* *K*-shell hole), the nondipole contributions

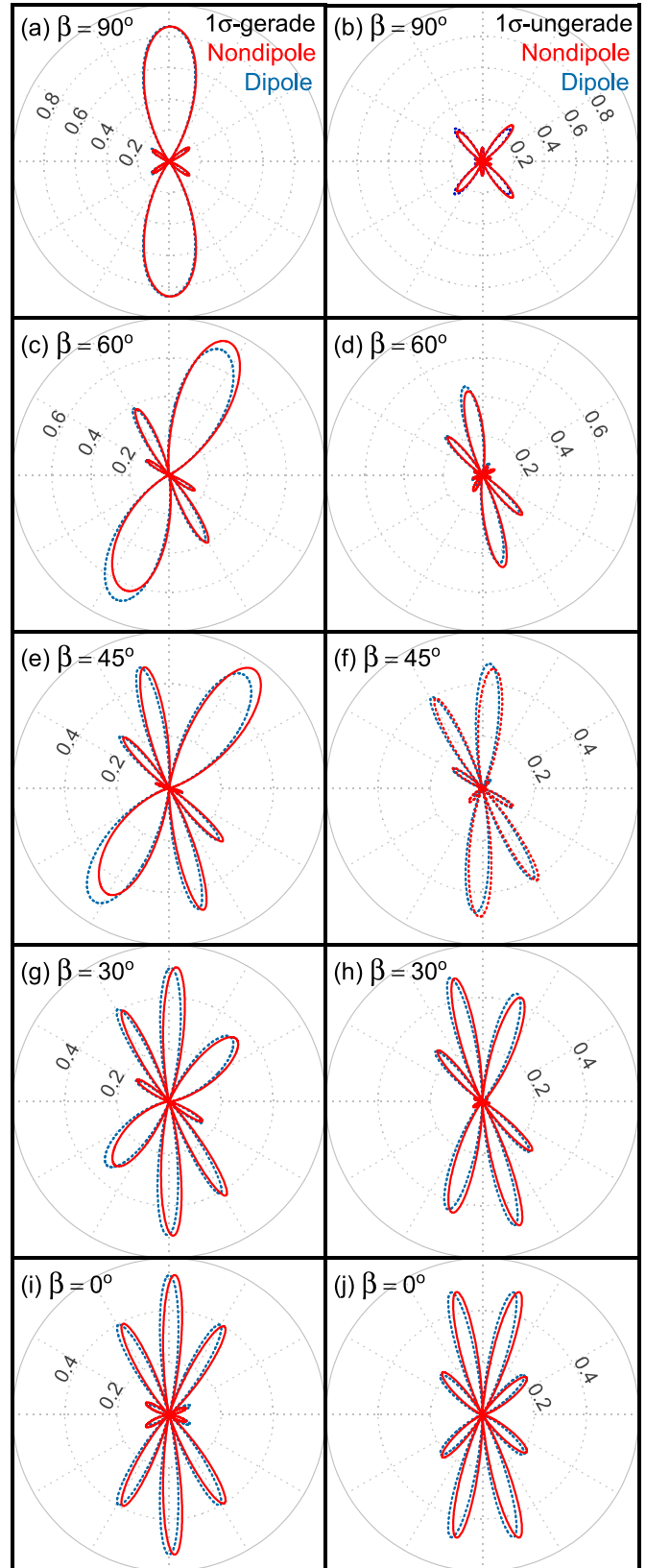


Figure 3. Theoretical angular emission distribution of the $1\sigma_g$ (left panels) and $1\sigma_u$ (right panels) photoelectrons of N_2 ionized by photons with an energy of 880 eV, as computed in different approximations. See the caption of figure 1 for details on the data representation and the scheme in figure 1(j) for the definition of the molecular orientation angle β .

act differently at different emission directions within each of the hemispheres. As one can see from the right panels of this figure, at preferable emission directions (i.e. for largest lobes), they increase the probability in the forward and decrease in the backward hemisphere, alike in the $1\sigma_g$ channel. However, this effect is opposite for the electrons emitted closely along the molecular axis, where the emission probability for the $1\sigma_u$ channel vanishes by symmetry. In a time-dependent perspective, the forward tilt of the central lobe in the $1\sigma_g$ channel in figure 3(i) can be attributed to a delay of the photoelectron birth time between the atom facing the incoming light as compared to the atom situated forward in the photon propagation direction, being caused by the travel time of the light between the two atomic centers [36].

4. Conclusion

We reported a continuation of our systematic study of the interplay between the molecular-potential scattering and nondipole effects in the core-shell photoemission from fixed-in-space molecules. Here, we demonstrate experimentally and theoretically how this interplay determines the final photoelectron emission distributions in homonuclear N_2 molecules at a photon energy of 880 eV. We observe that the nondipole effects break the symmetry of the main lobes in the photoemission, which are aligned along the molecular axis. In particular, the lobe which points along the light propagation direction becomes noticeably larger than the one pointing in the opposite direction. The effect emerges mainly in the $1\sigma_g$ photoionization channel, which is responsible for the emission probability along the molecular axis.



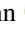





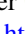

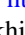

Data availability statement

All data that support the findings of this study are included within the article (and any supplementary files).

Acknowledgments

This work was supported by the Deutsche Forschungsgemeinschaft (DFG): experiment within the Project No. 447234583 (DO 604/38-1) and theory by the Project No. 492619011 (DE 2366/6-1). F T acknowledges funding by the Deutsche Forschungsgemeinschaft (DFG, German Research Foundation) - Project 509471550, Emmy Noether Programme. We acknowledge DESY (Hamburg, Germany), a member of the Helmholtz Association HGF, for the provision of experimental facilities. Parts of this research were carried out at PETRA III and we would like to thank the staff of beamline P04 for excellent support during the beamtime. Beamtime was allocated for proposal I-20180773. This research was supported in part through the Maxwell computational resources operated at DESY.

ORCID iDs

D V Rezvan  <https://orcid.org/0009-0008-0420-1893>
 A Pier  <https://orcid.org/0009-0007-1185-3016>
 S Grundmann  <https://orcid.org/0000-0001-6512-6921>
 N M Novikovskiy  <https://orcid.org/0000-0002-5781-1862>
 N Anders  <https://orcid.org/0000-0003-0458-6689>
 M Kircher  <https://orcid.org/0000-0002-1592-5706>
 N Melzer  <https://orcid.org/0000-0001-6263-623X>
 F Trinter  <https://orcid.org/0000-0002-0891-9180>
 M S Schöffler  <https://orcid.org/0000-0001-9214-6848>
 T Jahnke  <https://orcid.org/0000-0003-1358-5629>
 R Dörner  <https://orcid.org/0000-0002-3728-4268>
 Ph V Demekhin  <https://orcid.org/0000-0001-9797-6648>

References

- [1] Simon M, Piancastelli M N and Lindle D W 2016 *Hard-x-ray Photoelectron Spectroscopy of Atoms and Molecules Inhard x-ray Photoelectron Spectroscopy (Haxpes)* ed J C Woicik (Springer International Publishing Switzerland) pp 65–110
- [2] Krässig B, Jung M, Gemmell D S, Kanter E P, LeBrun T, Southworth S H and Young L 1995 *Phys. Rev. Lett.* **75** 4736
- [3] Lindle D W and Hemmers O 1999 *J. Electron Spectrosc. Relat. Phenom.* **100** 297
- [4] Dunford R W, Kanter E P, Krässig B, Southworth S H and Young L 2004 *Radiat. Phys. Chem.* **70** 149
- [5] Shigemasa E, Adachi J, Soejima K, Watanabe N, Yagishita A and Cherepkov N A 1998 *Phys. Rev. Lett.* **80** 1622
- [6] Underwood J G and Reid K L 2000 *J. Chem. Phys.* **113** 1067
- [7] Landers A et al 2001 *Phys. Rev. Lett.* **87** 013002
- [8] Grum-Grzhimailo A N 2003 *J. Phys. B* **36** 2385
- [9] Rezvan D V et al 2022 *Phys. Rev. Lett.* **129** 253201
- [10] Weber T et al 2001 *J. Phys. B* **34** 3669
- [11] Kaiser L et al 2020 *J. Phys. B* **53** 194002
- [12] Vela-Peréz I et al 2023 *Phys. Chem. Chem. Phys.* **25** 13784
- [13] Schöffler M S et al 2008 *Science* **320** 920
- [14] Brumboiu I E, Eriksson O and Norman P 2019 *J. Chem. Phys.* **150** 044306
- [15] Kircher M et al 2019 *Phys. Rev. Lett.* **123** 243201
- [16] Zimmermann B et al 2008 *Nat. Phys.* **4** 649
- [17] Hosaka K, Adachi J, Golovin A V, Takahashi M, Teramoto T, Watanabe N, Yagishita A, Semenov S K and Cherepkov N A 2006 *J. Phys. B* **39** L25
- [18] Toffoli D and Decleva P 2006 *J. Phys. B* **39** 2681
- [19] Viefhaus J, Scholz F, Deinert S, Glaser L, Ilchen M, Seltmann J, Walter P and Siewert F 2013 *Nucl. Instrum. Methods Phys. Res. A* **710** 151
- [20] Dörner R, Mergel V, Jagutzki O, Spielberger L, Ullrich J, Moshhammer R and Schmidt-Böcking H 2000 *Phys. Rep.* **330** 95
- [21] Ullrich J, Moshhammer R, Dorn A, Dörner R, Schmidt L Ph H and Schmidt-Böcking H 2003 *Rep. Prog. Phys.* **66** 1463
- [22] Zare R N 1972 *Mol. Photochem* **4** 1 (available at: <https://web.stanford.edu/group/Zarelab/publiclinks/zarepub60.pdf>)
- [23] Demekhin Ph V, Ehresmann A and Sukhorukov V L 2011 *J. Chem. Phys.* **134** 024113
- [24] Novikovskiy N M, Artemyev A N, Rezvan D V, Lagutin B M and Demekhin P V 2002 *J. Phys. B* **55** 175001
- [25] Huber K P and Herzberg G 1979 *Molecular Spectra and Molecular Structure. IV. Constants of Diatomic Molecules* (Springer Science + Business Media)

- [26] Schmidt M W *et al* 1993 *J. Comput. Chem.* **14** 1347
- [27] Dunning J T H 1971 *J. Chem. Phys.* **55** 716
- [28] Alagia M *et al* 2005 *Phys. Rev. A* **71** 012506
- [29] Starace A F 1982 *Theory of Atomic Photoionization Handbuch der Physik* vol 31 (Springer) pp 1–121
- [30] Kazama M, Shinotsuka H, Fujikawa T, Stener M, Decleva P, Adachi J-I, Mizuno T and Yagishita A 2012 *J. Electron Spectrosc. Relat. Phenom.* **185** 535
- [31] Cherepkov N A, Semenov S K, Hikosaka Y, Ito K, Motoki S and Yagishita A 2000 *Phys. Rev. Lett.* **84** 250
- [32] Semenov S K and Cherepkov N A 2002 *Phys. Rev. A* **66** 022708
- [33] Semenov S K *et al* 2006 *J. Phys. B* **39** 375
- [34] Rezvan D V, Novikovskiy N M, Martin L, Artemyev A N and Demekhin P V 2022 *Phys. Rev. A* **105** 033108
- [35] Rezvan D V, Novikovskiy N M, Haubenreißer D M, Lagutin B M and Demekhin P V 2023 *J. Phys. B* **56** 195003
- [36] Grundmann S *et al* 2020 *Science* **370** 339